CHEMISTRY OF MATERIALS

Article

pubs.acs.org/cm

Mechanistic Insights in Seeded Growth Synthesis of Colloidal Core/Shell Quantum Dots

Igor Nakonechnyi,[†,‡] Michael Sluydts,[¶] Yolanda Justo,[†,‡,§] Jacek Jasieniak,[∥] and Zeger Hens*[,†,‡]

[†]Physics and Chemistry of Nanostructures, Ghent University, Ghent, Belgium

[‡]Center for Nano and Biophotonics, Ghent University, Ghent, Belgium

[¶]Center for Molecular Modeling, Ghent University, Ghent, Belgium

[§]SIM vzw, Zwijnaarde, Belgium

[∥]Department of Materials Science and Engineering, Monash University, Melbourne, Victoria, Australia

Supporting Information

ABSTRACT: We analyze the mechanism of seeded growth reactions used to synthesize colloidal core/shell nanocrystals. Looking at the formation of CdSe/CdS and CdSe/ZnSe using both zinc blende and wurtzite CdSe seeds with a different surface termination, we show that the formation rate of the shell material does not depend on the presence of the seed nanocrystals. This suggests that shells grow by inclusion of CdS or ZnSe initially formed in the reaction mixture, possibly under the form of reactive monomers, and not by successive adsorption and reaction of metal and chalcogen precursors. This insight makes balancing homogeneous nucleation and heterogeneous growth of the shell material key to suppressing spurious secondary nucleation. Through a combination of experimental work and reaction simulations, we argue that this can be effectively achieved by raising the monomer solubility through the concentration of carboxylic acid used in the seeded growth reaction.

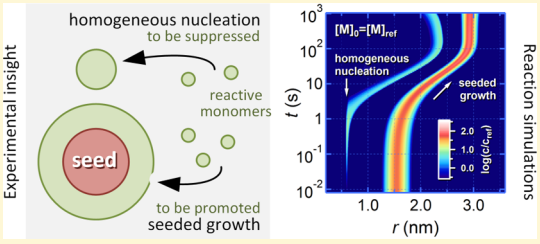

INTRODUCTION

Colloidal semiconductor nanocrystals or quantum dots (QDs) with a high photoluminescent quantum yield (PLQY) are currently studied for their possible use as, for example, remote phosphors in lighting and display applications, luminescent labels in bioimaging, or gain media in microlasers.[1] To achieve the necessary optoelectronic properties, QDs are commonly used under the form of core/shell structures, in which a shell with a commensurate crystal structure is grown over an original core QD. Such heteronanostructures have several advantages. First, wide band gap shell materials, such as ZnS, tend to passivate trap states at the core/shell interface and confine electron−hole pairs to the original core QD, a combination which can strongly enhance the QD PLQY.[2] Second, core/shell QDs with a staggered, so-called type II band alignment boast spatially separated electron−hole pairs that make possible a gamut of novel exciton phenomena, such as single exciton gain.[3] Finally, shell materials enhance the absorption cross-section of the resulting core/shell QDs at photon energies above their band gap transition. Here, CdS is particularly interesting since its 2.4 eV band gap makes for a selective boosting of the QD absorbance at wavelengths below ≈500 nm. This renders CdSe/CdS QDs an ideal downconverting phosphor for lighting and displays, which typically rely on a blue pump LED emitting at around 450 nm.[4]

Most shelling reactions rely on a two-step approach where core and shell are formed in successive stages.[5] In precursor-addition reactions, shelling is achieved through the addition of shell precursors to a reaction mixture containing the cores. To suppress homogeneous nucleation, precursors are typically added dropwise, either together or, to enforce layer-by-layer shell growth, one at the time.[6] Precursor-addition based shelling is therefore intrinsically slow and thus ill-suited for the formation of QDs with a large shell-to-core volume ratio, which is particularly useful for photoluminescent down-conversion. A considerably faster alternative is a seeded growth reaction, where shelling is achieved by launching a second hot injection synthesis, while coinjecting cores as seeds that act as heterogeneous nucleation centers. First developed as a method that promotes anisotropic growth, including dot-in-rods,[7−9] tetrapods,[10,11] or octapods,[12] the approach also proved most useful for the formation of quasi spherical core/shell QDs, where, e.g., thick CdS shells could be grown around core CdSe QDs in a matter of minutes.[13,14]

Following the establishment of protocols for the precision synthesis of several core QDs, various studies have addressed the chemistry of precursor conversion and the kinetics of nucleation and growth. Particularly for the case of CdSe QDs, this has led to an understanding that the actual precipitant is a homogeneously formed CdSe unit or *monomer*.[15,16] As a result, it was found that the monomer formation rate is a key factor in a hot injection synthesis, determining, for example the diameter

Received: January 26, 2017
Revised: May 19, 2017
Published: May 19, 2017

DOI: 10.1021/acs.chemmater.7b00354
Chem. Mater. 2017, 29, 4719−4727

of the QDs when the reaction reaches its final yield.[17−19] This finding has been successfully implemented for size-tuning-at-full-yield using precursors with different reactivity to form nanocrystals of a controlled size with a high reaction yield.[19] It is expected that similar considerations will apply to seeded growth shelling reactions. Such insights can help to determine the optimized reaction times, map conditions where homogeneous nucleation is best suppressed, and identify the general conditions that make reactions suited for seeded growth.[20] Such a mechanistic approach to shelling reactions, however, is absent in the current literature.

Here, we start from the seeded growth synthesis of CdSe/CdS core/shell QDs using zinc blende CdSe seeds to identify the key steps in such shelling reactions. We first show that the reaction conditions have a significant impact on the reaction outcome, especially with respect to the extent of secondary nucleation. Next, we analyze the time development of the reaction yield and show that the CdS formation rate is independent of the presence of CdSe seeds and the possible suppression of homogeneous nucleation. A similar finding is observed for the seeded growth of ZnSe on zinc blende CdSe cores and both CdS and ZnSe on wurtzite CdSe cores. We thus conclude that seeded growth reactions are fundamentally different from layer-by-layer growth procedures, in the sense that the reactive precursors do not adsorb at, and react one-by-one with, the seed QDs. Rather, our findings suggest that shells grow by the incorporation of monomers that first form homogeneously in solution. We implement this mechanistic picture in kinetic reaction simulations that were previously used to model hot injection syntheses involving homogeneous nucleation.[17] We find that the same reaction parameters that govern homogeneous nucleation and growth are key to steer the outcome of seeded growth reactions, where an increased monomer solubility helps to suppress homogeneous nucleation.

EXPERIMENTAL SECTION

Zinc Blende CdSe Core QDs. Zinc blende (zb) CdSe core quantum dots (QDs) were synthesized using the method first described by Flamee et al.[21] In brief, 0.5 mmol of CdO was mixed with 1.6 mmol of myristic acid and 10 mL of octadecene (ODE) after which the mixture was heated under ambient conditions until total dissolution at 260 °C. Next, 0.24 mmol of black Se, dispersed as a powder in 1-octadecene, was swiftly added to the solution, and after 5 min, the reaction was stopped by thermal quenching using a water bath. This yields zb-CdSe QDs having a first exciton peak absorption at 537 nm, corresponding to a mean diameter of about 3 nm.[22] The QDs were separated from the reaction mixture by addition of propanol-2 (1:1 in volume as compared to the reaction mixture) and centrifugation (here and afterward, centrifugation was done at a *g*-force of 3000*g*) to obtain a QD pellet. The QDs were redispersed in a mixture of 1 mL of toluene and 1 mL of oleic acid (OA) to replace the original myristate ligands by oleate. For seeded growth reactions, this core QD solution was further purified thrice using 1 mL of toluene and 1 mL of methanol as the solvent/nonsolvent combination. For what follows, the concentration of CdSe QDs was calculated using the average absorbance of a diluted sample at 300, 320, and 340 nm which is directly proportional to the volume fraction of CdSe.[22]

Wurtzite CdSe Core QDs. Wurtzite (wz) CdSe core quantum dots were synthesized using the method described by Drijvers et al.[14] In brief, 1.5 mmol of CdO was mixed with 6 mmol of TDPA, 24 mmol of oleyl alcohol, and 10 g of trioctylphosphine oxide (TOPO), heated until 120 °C, and kept under a nitrogen flow for 1 h. Afterward, the mixture was heated until 350 °C. When the solution became colorless, 2 mL of trioctylphosphine (TOP) was injected. After the temperature recovered, 1.5 mL of 2 M TOP-Se was injected. After ±5 s, the reaction mixture is quickly cooled by a preheated water bath. When the reaction mixture reached a temperature of ≈80 °C, 15 mL of MeOH was added and the destabilized dispersion was centrifuged for 1 min. Afterward, the core solution is purified thrice using 1 mL of hexane and 1 mL of ethanol as the solvent/nonsolvent combination.

zb-CdSe/CdS by Seeded Growth. zb-CdSe/CdS core/shell QDs were synthesized using a modification of the *flash* approach described by Cirillo et al.[13] In brief, 0.25 mmol of CdO, 5.6 mmol of OA, and 3.8 mL of ODE were loaded in a three-neck flask. The flask was first kept under a nitrogen flow for 1 h at 120 °C and then heated to 260 °C to form cadmium oleate. In the meanwhile, 50 nmoles of CdSe cores and 0.38 mL of a 2 M TOP-S solution were dissolved in 1.12 mL of ODE. After the complete dissolution of CdO, the solution containing the QD cores and the sulfur precursor was rapidly injected into the flask at 260 °C. Aliquots for chemical yield studies were taken after regular time intervals, 10 s, 30 s, 1 min, 1 min 30 s, 2 min, 3 min, 4 min, 5 min, and 6 min, and put in 1 mL of toluene. Samples for TEM were precipitated with ethanol and then purified thrice using 1 mL of hexane and 1 mL of ethanol as the solvent/nonsolvent combination.

zb-CdSe/ZnSe by Seeded Growth. zb-CdSe/ZnSe core/shell QDs were obtained using the same protocol as for CdSe/CdS. Here, 0.65 mmol of ZnO, 5.3 mmol of OA, and 3.8 mL of ODE were loaded in a three-neck flask. The flask was first kept under a nitrogen flow for 1 h at 120 °C and then heated to 310 °C to form zinc oleate. In the meanwhile, 25, 50, or 100 nmole of CdSe core QDs and 0.215 mL of a 2 M TOP-Se solution were dissolved in 1.285 mL of ODE. After the formation of zinc oleate, the solution containing the QD cores and the selenium precursor was rapidly injected into the flask at 260 °C. Aliquots for chemical yield studies were taken after 30 s, 1 min, 4 min, 8 min, 12 min, 18 min, 27 min, and 40 min and put in 1 mL of toluene. Samples for TEM where precipitated with ethanol and then purified thrice using 1 mL of hexane and 1 mL of ethanol as the solvent/nonsolvent combination.

wz-CdSe/CdS by Seeded Growth. wz-CdSe/CdS core/shell QDs were synthesized using a modification of the *flash* approach described by Drijvers et al.[14] In brief, 0.6 mmol of CdO, 2.5 g of TOPO, and 2.5 g of OA were loaded in a three-neck flask. Next to this, 100 nmole of dried wz-CdSe cores and 0.5 mmol of sulfur were dissolved in 1 mL of TOP. The CdO containing flask was first kept under a nitrogen flow for 1 h at 120 °C and then heated to 340 °C to form cadmium oleate. After the complete dissolution of CdO, 1 mL of TOP was injected. After the temperature was recovered, the solution containing the QD cores and the sulfur precursor was injected into the flask. Aliquots for chemical yield studies were taken after regular time intervals, 5 s, 30 s, 1 min, 2 min, 3 min, 4 min, 5 min, and 6 min, and added to 1 mL of toluene. Samples for TEM where precipitated with ethanol and then purified thrice using 1 mL of hexane and 1 mL of ethanol as the solvent/nonsolvent combination.

wz-CdSe/ZnSe by Seeded Growth. wz-CdSe/ZnSe core/shell QDs were obtained using the same protocol as for wz-CdSe/CdS. Here, 0.65 mmol of ZnO, 5.3 mmol of OA, and 3.8 mL of ODE were loaded in a three-neck flask. Next to this, 100 nmole of wz-CdSe core QDs and 0.96 mmol of Se were added to 1 mL of TOP. The flask containing the ZnO was first kept under a nitrogen flow for 1 h at 120 °C and then heated to 340 °C to form zinc oleate. After the formation of zinc oleate, 1 mL of TOP was injected. After the temperature was recovered, the solution containing the QD cores and the selenium precursor was rapidly injected into the flask. Aliquots for chemical yield studies were taken after 5 s, 1 min, 2 min 30 s, 5 min, 10 min, 20 min, 30 min, and 60 min and put in 1 mL of toluene. Samples for TEM where precipitated with ethanol and then purified thrice using 1 mL of hexane and 1 mL of ethanol as the solvent/nonsolvent combination.

Materials Characterization. UV−vis absorption spectra were taken with PerkinElmer Lambda 950 and Varian Cary 500 spectrophotometers. Samples for transmission electron microscopy (TEM) were prepared by dropcasting a solution on a carbon coated copper grid. Bright field TEM images were recorded using a Cs-corrected JEOL 2200 FS microscope. Photoluminescence emission spectra were performed with an Edinburgh Instruments FLS920 fluorescence spectrometer. The absolute PLQY of QD dispersions was

DOI: 10.1021/acs.chemmater.7b00354
Chem. Mater. 2017, 29, 4719−4727

measured with an integrating sphere (152 mm, Spectralon coated) connected to a CCD camera (Princeton Instruments ProEM 16002) and a spectrograph (Princeton Instruments Acton SP2358).

Chemical Yield Calculation. In general, the volume fraction f of QD material in a sample can be calculated from the QD absorbance A, provided the intrinsic absorption coefficient μ_i of the QDs is known:[23]

$$f = \frac{\ln 10 \times A}{\mu_i} \quad (1)$$

This equation also applies to core/shell QDs, yet in this case, μ_i depends on the relative volume of core and shell, a ratio that is a priori unknown in a given sample and that changes during a seeded growth reaction. However, for two materials with relatively similar optical constants, the intrinsic absorption coefficient $\mu_{cls,i}$ of a core/shell QD can be seen as a linear combination of the intrinsic absorption coefficient of core ($\mu_{c,i}$) and shell ($\mu_{c,s}$); a relation that applies for example to CdSe/CdS core/shell QDs.[24] Hence, writing the volume ratio V_s/V_{cls} as ϕ, $\mu_{cls,i}$ thus reads:

$$\mu_{cls,i} = \phi\mu_{s,i} + (1 - \phi)\mu_{c,i} \quad (2)$$

The volume fraction of core/shell QDs f_{cls} in a dispersion can thus be calculated from their absorbance A_{cls} as:

$$f_{cls} = \frac{\ln 10 \times A_{cls}}{\mu_{cls,i}}$$

Since the volume fractions f_s and f_c of shell and core material equal ϕf_{cls} and $(1-\phi)f_{cls}$, respectively, this expression can be rewritten using eq 2 as

$$f_s\mu_{i,s} + f_{i,c}\mu_{i,c} = \ln 10 \times A_{cls}$$

Hence, the volume fraction f_s can be obtained as

$$f_s = \frac{\ln 10 \times (A_{cls} - A_c)}{\mu_{i,s}} \quad (3)$$

In this manuscript, the chemical yield of seeded growth reactions is always estimated by means of eq 3 using the following values for $\mu_{i,s}$ at 320 nm in the case of zb-CdS and zb-ZnSe and at 300 nm in the case of wz-CdS:

$$\mu_{i,\text{zb-CdS}} = 1.56 \times 10^5 \text{cm}^{-1} \quad (4)$$

$$\mu_{i,\text{zb-ZnSe}} = 1.15 \times 10^5 \text{cm}^{-1} \quad (5)$$

$$\mu_{i,\text{wz-CdS}} = 1.73 \times 10^5 \text{cm}^{-1} \quad (6)$$

These numbers were calculated from the bulk optical constants of CdS and ZnSe,[25] following a previously published methodology.[23] Since no data on the optical constants of wurtzite ZnSe are available, optical constants for zinc blende ZnSe were used instead.

Absorbance spectra were always measured on unpurified samples. To correct for the presence of absorbing species, such as OA and ODE, we therefore calculated f_s by subtracting the absorbance of the first aliquot from the absorbance of any other aliquot instead of a mere correction for A_c as expressed by eq 3. Clearly, this leads to a small underestimation of the amount of shell material formed. From f_s, the volume of shell material V_s in each aliquot is then obtained as the product of f_s and the aliquot volume V:

$$V_s = f_s \times V$$

Finally, the amounts of cations and anions in the shell are obtained from V_s, the number of atoms per unit cell n, and the unit cell volume V_{uc} of the respective material as:

$$n_{cat} = \frac{nV_sN_A}{V_{uc}} \times \frac{\nu}{1 + \nu} \quad (7)$$

$$n_{an} = \frac{nV_sN_A}{V_{uc}} \times \frac{1}{1 + \nu} \quad (8)$$

Here, ν stands for the actual cation/anion ratio in the nanocrystals analyzed. Depending on the yield limiting reagent, a chemical yield is then obtained from the ratio between the amount of cations or anions in the aliquot and the amount initially used in the synthesis.[19,21,26] Note that in this work, all yield calculations have been done assuming stoichiometric nanocrystals (ν = 1). While this is in general not true, the error in the calculated numbers that results from neglecting the nonstoichiometry is small and the assumption does not invalidate the conclusions we draw from the yield development in this work.

EXPERIMENTAL RESULTS

Heterogeneous versus Homogeneous Nucleation. To obtain first insights in the mechanism of seeded growth reactions, we started this investigation with syntheses that use oleate-capped zinc blende (zb) CdSe nanocrystals as seeds around which a CdS shell is grown using cadmium oleate as the cadmium precursor. In this way, possible side effects linked to changes in surface termination could be avoided. Figure 1a depicts a series of absorption spectra recorded on aliquots taken at different times after initiating this seeded growth of CdS on zb-CdSe core QDs following the procedure as described in the Experimental Section and using an oleic acid (OA) to Cd molar ratio of 20:1. To simplify the interpretation, all spectra have been normalized to the mass of the aliquot taken, so the absorbance at short wavelength is directly proportional to the amount of inorganic material formed in the reaction. Whereas the first aliquot mainly shows an additional UV absorbance due to the remaining reagents (see Experimental Section), from the second aliquot, the spectra exhibit an additional, yet featureless absorbance that extends from UV wavelengths up to ≈520 nm; a wavelength corresponding to the band gap of bulk CdS. In addition, the CdSe first exciton transition shows a marked redshift with increasing reaction time, which is a well-known characteristic of CdSe/CdS core/shell QDs. Both the additional absorption at shorter wavelengths and the red shift of the

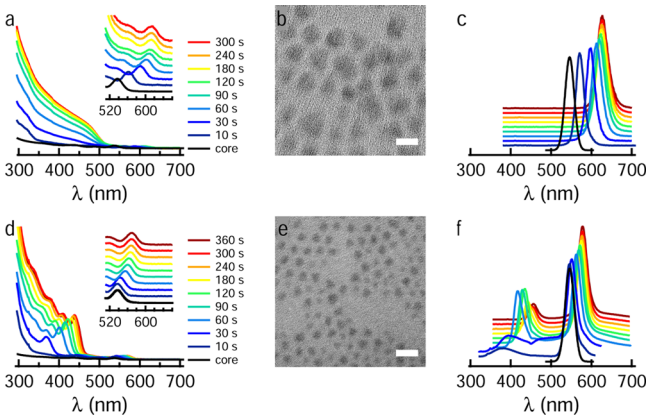

Figure 1. (a) Series of absorption spectra recorded on (black) the original CdSe core QDs and (colored curves) aliquots taken at the moment indicated by the legend after starting a CdSe/CdS seeded growth synthesis run using a 20:1 oleic acid (OA)/Cd molar ratio. All spectra have been normalized using the mass of the respective aliquot. (b) Bright field TEM image of the reaction product obtained after 2 min of reaction. Scale bar is 10 nm. (c) Photoluminescence spectrum of the CdSe core QDs and all reaction aliquots corresponding to the absorption spectra shown in (a). (d–f) The same as (a–c) for a CdSe/CdS seeded growth reaction run using a OA/Cd ratio of 3:1.

DOI: 10.1021/acs.chemmater.7b00354
Chem. Mater. 2017, 29, 4719–4727

exciton absorption level off after about 120 s, suggesting that the CdS formation reaction reaches its final yield within this time span. Importantly, no changes of the absorption spectra were observed in blank reactions where CdSe core QDs are injected while removing one or both reactive precursors (see Supporting Information S1).

The transmission electron microscopy (TEM) image shown in Figure 1b confirmed that the reaction resulted in the formation of relatively large (<*d*> = 8.6 nm ± 1.5 nm) nanocrystals out of the initial 3.1 nm zb-CdSe core QDs with an overall zinc blende structure (see Supporting Information S2). It can be seen that this conclusion is corroborated by the photoluminescence spectra of the aliquots (see Figure 1c). All spectra contain a single, narrow emission peak that shifts to longer wavelengths with respect to the original CdSe photoluminescence in accordance with the red shift of the first exciton transition in the absorption spectra. We typically found a photoluminescence quantum yield (PLQY) of CdSe/CdS core/shell QDs formed using zb-CdSe seeds of about 30−35% (see Table 1). While this figure is comparable to what is reported for CdSe/CdS formed using layer-by-layer shell growth,[6] it is moderate as compared to, for example, CdSe/CdS heteronanocrystals formed through seeded growth around wurtzite CdSe cores.[14]

Table 1. Overview of Structural and Optical Properties of the Different Core/Shell Nanocrystal Systems Analyzed Here[a]

core/shell	d_{core} (nm)	d_{shell} (nm)	PLQY (%)
zb-CdSe/CdS	3.1	8.6 ± 1.5	35
zb-CdSe/ZnSe	3.1		55
wz-CdSe/CdS	3.4	11.2 ± 2.3	60
wz-CdSe/ZnSe	3.6	11.2 ± 1.4	80

[a] d_{core}: core diameter; d_{shell}: shell thickness. Given the ill-defined shape of the zb-CdSe/ZnSe heteronanocrystals, no thickness is given.

The reaction outcome changed when the OA/Cd ratio in the seeded growth reaction was lowered to 3:1, keeping all other reaction parameters constant. Under these conditions, the additional CdS absorbance in the successive absorbance spectra contains pronounced features and exhibits a progressive red shift with increasing reaction time (see Figure 1d). Moreover, the CdSe first exciton transition only shifts to 570 nm, a value already reached by the first aliquot in the 20:1 reaction. Both elements point toward the formation of additional CdS quantum dots by secondary nucleation. The TEM images of the end product shown in Figure 1e confirm this conclusion, since they represent a set of QDs with a broad size distribution that are all significantly smaller than the QDs formed by the 20:1 reaction. Evidence of the simultaneous occurrence of secondary nucleation and CdS shell growth can also be found in the photoluminescence spectra of the aliquots, which show two emission lines (see Figure 1f). Here, the long wavelength line clearly corresponds to the emission of the original CdSe cores, gradually shifting to longer wavelengths due to CdS shelling, whereas the second, short wavelength line is related to newly formed CdS quantum dots that grow larger with increasing reaction time.

In Figure 2, we represent the absorption and photoluminescence spectra of aliquots taken during a similar seeded growth reaction, where ZnSe was formed in the presence of CdSe seeds. While changes to the absorption spectrum take much longer in this case, their overall evolution is similar to what we observed in the 20:1 reaction used to form CdSe/CdS core/shell QDs. As can be seen in Figure 2a, later aliquots exhibit an enhanced absorbance that contains little features and extends to ≈430 nm, a wavelength only slightly shorter than what is expected for bulk ZnSe. In this case, the first exciton transitions shift only slightly and the photoluminescence spectra show no indication of ZnSe nanocrystals being formed. Although TEM images demonstrate that this reaction results in rather irregular nanocrystals (see Figure 2c) with a zinc blende structure (see Supporting Information S2), it confirms the heterogeneous growth of ZnSe around the original zb-CdSe nanocrystals, possibly with a preference for specific facets. Notwithstanding their irregular shape, the zb-CdSe/ZnSe QDs formed by seeded growth featured a PLQY of 55% (see Table 1).

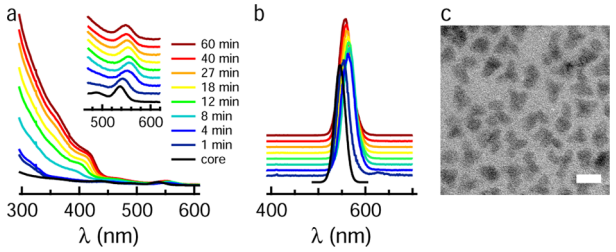

Figure 2. (a) Series of absorption spectra recorded on (black) the original CdSe core QDs and (colored curves) aliquots taken during a CdSe/ZnSe seeded growth synthesis run using a 20:1 oleic acid (OA)/Zn molar ratio. All spectra have been normalized using the mass of the respective aliquot. (b) Corresponding photoluminescence spectra; the same color coding as in (a) applies. (c) Bright field TEM image of the reaction product obtained after 60 min of reaction. Scale bar is 10 nm.

Chemical Yield Development. To get experimental insight in the kinetics of seeded growth reactions, we analyzed the yield of CdS and ZnSe formed as a function of time by means of the absorbance *A* of quantitative reaction aliquots according to the procedure outlined in the Experimental Section (eq 3). Focusing first on seeded growth of CdS, Figure 3a represents the thus calculated CdS yield for three different reactions. Note that yield in this case is determined as the ratio between the number of moles of CdS formed and of cadmium oxide used in the seeded growth reaction since the latter is the limiting reagent. Two reactions correspond to the 20:1 and 3:1 equiv of CdSe/CdS synthesis discussed in the previous section,

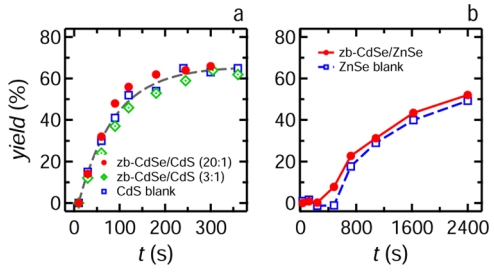

Figure 3. (a) Chemical yield development of CdSe/CdS seeded growth reactions under conditions of (filled red circles) 20:1 OA/Cd ratio, (green dotted diamonds) 3:1 OA/Cd ratio, and (open blue squares) no coinjection of seeds. The dashed gray line is a guide to the eye. (b) Chemical yield development of CdSe/ZnSe seeded growth reactions in the (filled red circles) presence of CdSe seeds and (open blue squares) without coinjection of seeds.

DOI: 10.1021/acs.chemmater.7b00354
Chem. Mater. 2017, 29, 4719−4727

whereas the third is a blank reaction where CdS formation is initiated in the absence of any CdSe seeds. It can be seen that all three reactions have the same yield development, where CdS formation runs to completion after ≈200 s of reaction time. This is a most remarkable result. It indicates that the rate of CdS formation is independent from the presence or absence of CdSe seeds or, in other words, on the nucleation regime: homogeneous, heterogeneous, or mixed. Note that the leveling off of the estimated yield at 60−70% may be due to an overestimation of the intrinsic absorption coefficients, which is often found when using calculated numbers based on bulk optical constants.[24]

Thinking of seeded growth reactions of a binary compound such as CdS, two different reaction pathways can be put forward. In the first, the Cd and S precursor react separately with the CdSe seed present. Such a set of half-reactions is known from so-called SILAR or colloidal ALD reactions, where they are effectively separated in time.[6,27] Alternatively, the Cd and S precursor, when injected together, could first react to form a Cd−S monomer that serves as the actual precipitant. Such a process is known to drive homogeneous nucleation in hot injection reactions, most notably in the formation of CdSe nanocrystals.[15] The finding that the CdS formation rate is independent of the nucleation regime clearly supports the latter pathway, where the formation rate of the Cd−S monomer dictates the overall formation rate of CdS. Interestingly, the same hypothesis was recently put forward as the mechanism behind shell growth in a SILAR reaction.[28] Even so, a yield analysis does not give evidence as to what CdS entity binds to the CdSe cores, an actual Cd−S monomer or larger CdS clusters. While the lack of photoluminescence of small CdS quantum dots (see Figure 1) and the absence of tiny clusters in the TEM images suggest that shell growth involves monomer adsorption, it should be clear that shell growth through the binding of larger CdS clusters to the core QDs cannot be ruled out.

Figure 3b shows the same yield development analysis for the case of ZnSe growth, in the presence or absence of CdSe seeds. In this case, the shell growth is considerably slower, reaching a yield of almost 50% after 40 min. Moreover, it appears that homogeneous nucleation is significantly delayed since ZnSe nanocrystals are only apparent in the absorbance spectra approximately 500 s after the start of the reaction. This delay can be interpreted as the time the reaction needs before the monomer concentration attains the supersaturation needed for homogeneous nucleation to start, possibly due to a combination of a slow monomer formation and a relatively high monomer solubility. With CdSe seeds present, this nucleation delay is markedly shorter, but an otherwise highly similar yield development is obtained. Again, this corresponding yield development points toward a reaction pathway where ZnSe monomers bind to CdSe seeds. In this respect, the reduction of the ZnSe formation delay then represents the reduced supersaturation for heterogeneous nucleation.

Seeded Growth with Wurtzite CdSe Cores. To further explore the general character of the observation that the growth rate of the shell in a seeded growth reaction is set by the rate at which monomers of the shell material are formed, we extended the analysis to CdSe/CdS and CdSe/ZnSe heteronanocrystals formed by the injection of wurtzite (wz) CdSe nanocrystals as seeds. Focusing first on CdSe/CdS, Figure 4a−c gives a series of absorption and photoluminescence spectra and the concomitant yield of CdS formation as recorded on aliquots

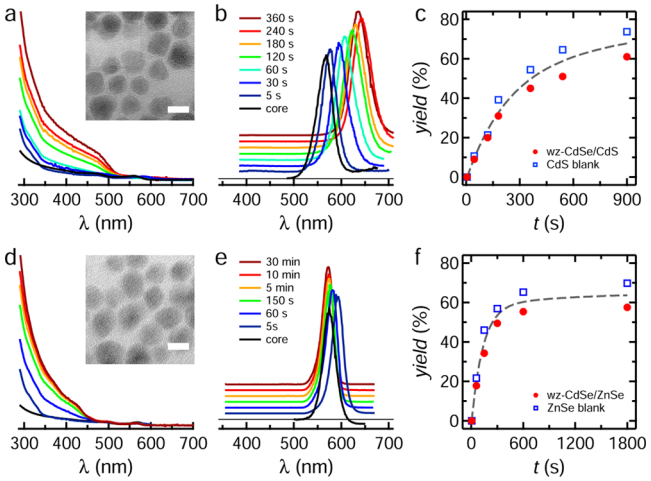

Figure 4. (a) Series of absorption spectra recorded on (black) the original CdSe core QDs and (colored curves) aliquots taken at moments as indicated after starting a wz-CdSe/CdS seeded growth synthesis. All spectra have been normalized using the mass of the respective aliquot. (Inset) Bright field TEM image of the reaction product obtained after 2 min of reaction. Scale bar is 10 nm. (b) Photoluminescence spectra of the wz-CdSe core QDs and all reaction aliquots corresponding to the absorption spectra shown in (a). (c) Chemical yield development of (closed red circles) a wz-CdSe/CdS seeded growth reaction and (open blue squares) the corresponding blank reaction. The dashed gray line is a guide to the eye. (d−f) The same as (a−c) for a wz-CdSe/ZnSe seeded growth reaction.

taken at different times after initiating the seeded growth reaction (see Experimental Section for more details). Note that, in this case, we immediately used the condition of high oleic acid concentration that is known to reduce homogeneous CdS nucleation.[13] Although the rate of CdS formation is different for this *flash* synthesis, the overall picture that emerges is highly similar to the case of zb-CdSe/CdS. Again, a largely featureless CdS absorption shows up and the band gap absorption and emission exhibit the redshift characteristic of CdS shelling. This is confirmed by the TEM image represented in Figure 4a, which shows that the originally 3 nm wz-CdSe seeds are turned into ∼10 nm quasi-spherical nanocrystals with a wurtzite structure (see Supporting Information S2). As shown previously, the wz-CdSe seed nanocrystals used here are terminated by phosphonate and phosphonate anhydride ligands.[29] In spite of this different surface chemistry, Figure 4c shows that the yield of CdS formation in reactions with and without seeds is nearly identical; a result similar to what we found with zb-CdSe seeds terminated by oleate ligands. This observation further confirms the conclusion that CdS formation is not surface catalyzed, but is dictated by the same CdS monomer formation reaction in the blank synthesis and the seeded growth reaction.

Figure 4d−f represents a similar data set for a seeded growth synthesis of CdSe/ZnSe core/shell nanocrystals using wz-CdSe cores. Similar reaction conditions as for wz-CdSe/CdS seeded growth were used, yet the Cd and S precursors were replaced by the concomitant Zn and Se precursors. In agreement with the formation of zb-CdSe/ZnSe, the largely featureless contribution of ZnSe to the absorption spectrum can be discerned in the reaction aliquots, in this case already in the 60 s aliquots, and the peak wavelengths of the exciton absorption and emission remain essentially constant. On the other hand, TEM micrographs attest to the formation of quasi-spherical nanocrystals with a wurtzite structure (see Supporting

DOI: 10.1021/acs.chemmater.7b00354
Chem. Mater. 2017, 29, 4719−4727

Information S2), where the increase in diameter as compared to the ZnSe seeds further confirms the formation of core/shell heteronanocrystals (see Table 1). Moreover, the wz-CdSe/ZnSe QDs formed here using a seeded growth *flash* procedure have a PLQY of 80%, a remarkably high number since no further ZnS overcoating nor postsynthesis annealing was used.[30,31] Also in this case, we find a highly similar development of the reaction yield with time when comparing ZnSe formation without and with the coinjection of wz-CdSe seeds (see Figure 4f).

Kinetic Modeling of Seeded Growth Reactions. Knowing the two-step character of seeded growth reactions, such reactions can be explored using kinetic reaction simulations as previously developed to assess hot injection syntheses of colloidal nanocrystals (NCs) based on in situ formation of a precipitant and homogeneous nucleation.[17] Note that we will henceforth use the more general term nanocrystals since these simulations are not necessarily restricted to the synthesis of quantum dots. Either way, such simulations make use of a kinetic scheme where the injected precursors P first react to form monomers M,[15,16] which are then used for either nucleation of new nanocrystals or growth of existing nanocrystals:

$$\text{Monomer formation} \quad \mathrm{P} \rightarrow \mathrm{M} \tag{9}$$

$$\text{Nucleation} \quad n^{\star}\mathrm{M} \rightarrow \mathrm{NC}_{n^{\star}} \tag{10}$$

$$\text{Growth} \quad \mathrm{M} + \mathrm{NC}_{n} \rightarrow \mathrm{NC}_{n+1} \tag{11}$$

Here, the subscript n denotes a NC made up of n monomers. Moreover, in line with classical nucleation theory, nucleation is described by eq 10 as a process where a stable nucleus is formed out of a critical number of monomers $n^{\star}$. As outlined in Supporting Information S3, the 3 reaction equations lead to 3 coupled differential equations. These describe the time dependence of the precursor and monomer concentration and of the nanocrystal concentration distribution $c(r,t)$, where $c(r,t)\Delta r$ yields the concentration of NCs with a radius in the range of $[r, r + \Delta r]$ at time t.

Figure 5a represents $c(r,t)$ as a t vs r color map for a hot injection synthesis simulation in the absence of seeds, a simulation that we will take as a reference in this work. The simulation implements a first order monomer formation reaction with a 3/100 s^{-1} rate constant, a low monomer solubility, and a close to diffusion limited growth (see Supporting Information S3). As can be seen in Figure 5a, this makes nucleation occur almost instantaneously upon injection. As more NCs are formed, growth becomes ever more important as an alternative monomer consumption pathway. This eventually leads to the complete suppression of NC nucleation, which we characterize as the moment where the NC concentration is maximal, followed by a rapid increase of the NC diameter that is driven by the continuous formation of new monomers. This reaction driven growth regime turns into a ripening driven regime after ≈100 s, the moment when the initial precursors are depleted. The same series of events can be recognized in Figure 5b, where the total NC concentration and the average radius are plotted as a function of reaction time.

As shown by the experimental work presented here, the initial presence of seed NCs does not fundamentally alter the reaction mechanism. Precursors are still converted into monomer species, which can be used to either grow existing NCs or nucleate new NCs. In this respect, seeded growth can

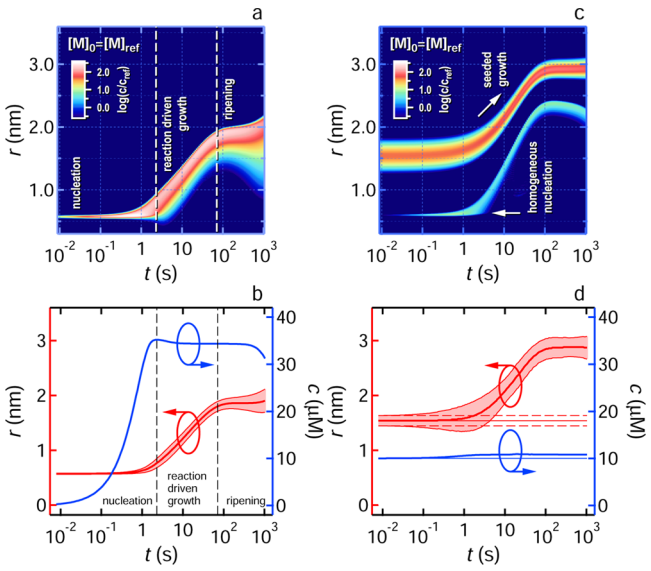

Figure 5. (a) Color map of the concentration distribution $c(r,t)$ for a simulated precursor-only hot injection synthesis (see Supporting Information S1 for parameter settings). (b) Time development of (blue) the nanocrystal concentration, (central red line) the average nanocrystal, and (top/bottom red line) the average nanocrystal radius plus or minus one standard deviation during the simulated precursor-only hot injection synthesis shown in (a). (c) Color map of the concentration distribution $c(r,t)$ for a simulated seeded growth synthesis using identical settings as for (a). (d) Time development of (blue) the nanocrystal concentration, (central red line) the average nanocrystal, and (top/bottom red line) the same plus or minus one standard deviation during the simulated synthesis shown in (c). The horizontal lines indicate the concentration and average radius of the seeds. In (a) and (c), colors refer to the logarithm of $c(r,t)/c_{ref}$ with c_{ref} equal to 1 μM·nm^{-1}.

be simulated using the same set of differential equations, yet changing the initial concentration distribution $c(r,0)$. An example is shown in Figure 5c,d. For this simulation, we kept all simulation parameters at their reference value and modeled $c(r,0)$ as a Gaussian distribution, characterized by an average radius of 1.54 nm, a size dispersion of 6%, and a total concentration of 10 μM. This initial distribution is clearly visible at early timepoints in the concentration map. Moreover, it can be seen that in this case a bimodal size distribution develops, which represents the combined effect of seeded growth and homogeneous nucleation (see Figure 5c). As shown in Figure 5d, the effect of homogeneous nucleation can be seen in the limited increase of the NC concentration by about 7.5% and the markedly deteriorated size dispersion reflecting the bimodal distribution.

The key to understand the outcome of the reaction simulations is the competition between nucleation and growth as two monomer consumption pathways. In this respect, nucleation is conveniently expressed through the nucleation rate J_N, defined as the number of NCs formed per unit volume and unit time:

$$J_N = \frac{2D}{v_0^{5/3}} \exp\left(-\frac{16\pi\gamma^3 V_m^2 N_A}{3(RT)^3(\ln S)^2}\right) \tag{12}$$

Here, D is the monomer diffusion coefficient, v_0 is the monomer volume, γ is the surface tension of a NC, V_m is the molar volume of the NC material, R is the gas constant, S is the monomer supersaturation, N_A is Avogadro's number, and T is

DOI: 10.1021/acs.chemmater.7b00354
Chem. Mater. 2017, 29, 4719−4727

the absolute temperature. Growth on the other hand can be characterized through the NC growth rate j_G, which is defined as the rate of change of the NC radius. Following Talapin et al.,[32] we write the growth rate as ($[M]_0$, monomer solubility; k_g^∞, monomer adsorption rate constant on a flat surface; α, transfer coefficient of the crystal growth reaction):

$$j_G = DV_m[M]_0\left[\frac{S - \exp\left(-\frac{2\gamma V_m}{rRT}\right)}{r + \frac{D}{k_g^\infty}\exp\left(\alpha\frac{2\gamma V_m}{rRT}\right)}\right] \quad (13)$$

Under the assumption of a constant, size-independent surface tension during the nucleation and growth stages, eqs 12 shows that J_N depends on the supersaturation S. In the initial stage of a hot injection synthesis, when monomer production has started but no nanocrystals have formed yet, the nucleation rate must match the monomer generation rate. This equality determines the critical supersaturation, and thus the critical radius, where nucleation occurs. The consumption of monomers by growth, on the other hand, depends on the concentration of NCs and the growth rate per NC j_G. Since the dominant term in j_G scales with the product of S and the solubility $[M]_0$, this being equal to the monomer concentration, the takeover of nucleation by growth will depend on the solubility. A high solubility promotes growth and causes an early nucleation/growth takeover, whereas a low solubility restricts growth and results in a late takeover.[33]

The same concept of favoring growth over nucleation can be applied to suppress homogeneous nucleation in a seeded growth reaction. In this case, all monomers produced can be consumed by growth from the very beginning of the reaction. To see whether this will occur, it is again useful to consider the critical supersaturation, this being the supersaturation that is needed for nucleation to consume all monomers produced. If consumption by growth would be much larger at the critical supersaturation than the monomer supply, growth will effectively prevent the reaction from reaching this nucleation threshold and nucleation can be suppressed. On the other hand, if monomer consumption by growth is small as compared to the monomer formation at the critical supersaturation, considerable nucleation will still occur. Since the growth rate at this critical supersaturation scales, for example, with the monomer solubility, this quantity is once more an effective parameter to tune a seeded growth reaction and suppress homogeneous nucleation.

On the basis of the idea that the monomer solubility is a straightforward way to suppress secondary nucleation, Figure 6a–d represents the outcome of seeded growth simulations using a 4-fold reduced and a 4-fold increased monomer solubility. As anticipated, lowering the solubility reduces the initial monomer consumption by seeded growth, which strongly enhances secondary nucleation. The NC concentration increases 8-fold, and the average diameter is largely determined by the contribution of the newly formed nanocrystals; see Figure 6b. Raising the solubility, on the other hand, brings the seeded growth reaction into a regime where secondary nucleation is effectively suppressed; see Figure 6c. As shown in Figure 6d, the original NC concentration stays constant and the seeds follow a pronounced reaction-driven growth trajectory, approximately doubling their radius.

Experimentally, we find that whether secondary nucleation occurs or not depends on the concentration of oleic acid added to the reaction mixture. At low acid concentration, the CdSe

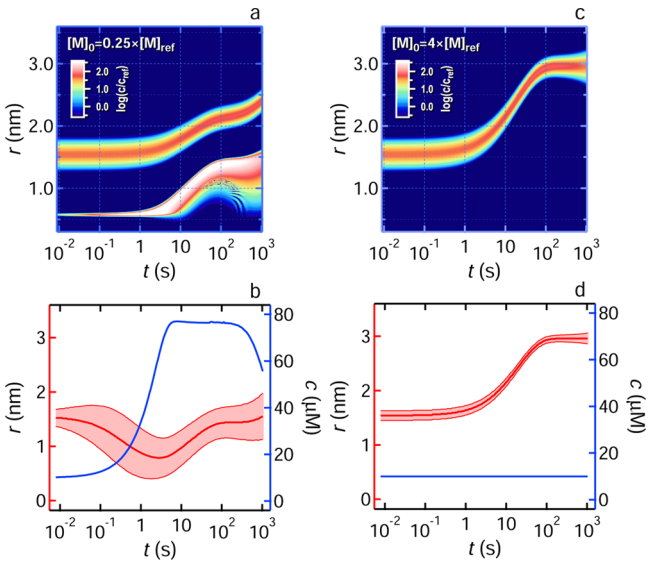

Figure 6. (a, c) Color map of the concentration distribution $c(r,t)$ for a simulated seeded growth synthesis where the monomer solubility is (a) reduced to a quarter of the reference value and (c) increased 4-fold as compared to the reference value. Colors refer to the logarithm of $c(r,t)/c_{ref}$ with c_{ref} equal to 1 μM·nm^{-1}. (b, d) Time development of (blue) the nanocrystal concentration, (central red line) the average nanocrystal, and (top/bottom red line) the same plus or minus one standard deviation during the simulated synthesis shown in (a) and (c), respectively.

seeds hardly grow and absorption and photoluminescence spectra attest the formation of CdS NCs. An approximately 6-fold increase of the acid concentration results in the complete suppression of CdS NC formation. Already, for a homogeneous hot injection synthesis, the influence of the acid concentration on the outcome of the synthesis was interpreted as promoting growth over nucleation and rationalized by relating higher acid concentrations to higher monomer solubilities.[33] As shown by Figure 6, the effect of a higher acid concentration on suppressing secondary nucleation in a seeded growth reaction can be accounted for in the same way. When growth is accelerated, for example, by increasing the acid concentration, a seeded growth reaction can indeed be driven into the desired growth-only regime. In this respect, it is useful to mention that the experimental variation of the acid concentration and the tuning range of the solubility in the reaction simulations are comparable for the hot injection synthesis studied before and the seeded growth reaction analyzed here. While this by itself does not prove our interpretation that the acid concentration is linked to the monomer solubility, nor give any experimental value to the simulation parameters, it does attest to the consistency of the interpretation. Indeed, in both cases, comparable changes in acid concentration in real reactions and monomer solubility in reaction simulations have the same effect on the NC growth rate.

The simulations used here model the growth rate by assuming that the NCs are spherical. On the other hand, seeded growth reactions have been widely used to form anisotropic NCs, such as CdSe/CdS dot-in-rods. However, our results suggest that also, in such cases, the rate at which shell material is formed depends on the rate of monomer formation and will be identical in blank reactions that contain no seed NCs. In fact, this point is illustrated by the zb-CdSe/ZnSe NCs (see Figure 2). While their morphology is far from spherical, the

DOI: 10.1021/acs.chemmater.7b00354
Chem. Mater. 2017, 29, 4719–4727

ZnSe formation rate is similar to that of the concomitant blank reaction. This implies that the trade-off between seeded growth and homogeneous nucleation that follows from the reaction simulations does not depend on the assumption that the NCs have a spherical shape. Hence, also in the case of anisotropic growth, shifting the balance between nucleation and growth, for example, by adjusting the monomer solubility, will be an effective strategy to suppress homogeneous nucleation.

CONCLUSION

Taking the examples of CdS and ZnSe shell growth around zinc blende and wurtzite CdSe seed quantum dots, we have shown that hot-injection seeded growth reactions follow a two-step mechanism. As the rate of CdS or ZnSe formation is independent of the presence of the CdSe seeds, shells grow by incorporating homogeneously formed CdS or ZnSe, probably as monomer species in the reaction mixture, and not by the successive adsorption and reaction of metal and chalcogen precursors. Kinetic simulations of this seeded growth mechanism indicate that heterogeneous growth rates must be sufficiently large to suppress the homogeneous nucleation of separate nanocrystals. In the case of CdSe/CdS formation, we show experimentally that whether secondary nucleation is suppressed or not depends on the free carboxylic acid in solution. Through simulations, this observation can be understood as the effect of an increased monomer solubility at high acid concentration, which favors heterogeneous growth over homogeneous nucleation. The insights provided by this work, both at the level of practical conditions for and conceptual understanding of seeded growth reactions, will be most useful to further the formation of complex hetero-nanocrystals by seeded growth methods.

ASSOCIATED CONTENT

Supporting Information

The Supporting Information is available free of charge on the ACS Publications website at DOI: 10.1021/acs.chemmater.7b00354.

Data on blank seeded growth reactions, the crystal structure of core/shell quantum dots, and an overview of the equations and parameters used in the kinetic reaction modeling (PDF)

AUTHOR INFORMATION

Corresponding Author

*E-mail: zeger.hens@ugent.be.

ORCID

Igor Nakonechnyi: 0000-0003-3955-2833
Michael Sluydts: 0000-0003-2798-3257
Zeger Hens: 0000-0002-7041-3375

Notes

The authors declare no competing financial interest.

ACKNOWLEDGMENTS

Z.H. acknowledges support by the European Comission via the Marie-Sklodowska Curie action Phonsi (H2020-MSCA-ITN-642656), the Belgian Science Policy Office (IAP 7.35, photonics@be), SIM vzw (SBO-APSYNC), IWT-Vlaanderen (SBO-Lumicor), and Ghent University (GOA no. 01G01513) for funding. I.N. acknowledges support by the European Comission via Erasmus Mundus Action 2 EUROEAST (EURO1300995) and Flanders Innovation & Entrepreneurship (VLAIO) (Innovation Mandate no. 150736, Swing).

REFERENCES

(1) Kovalenko, M. V.; Manna, L.; Cabot, A.; Hens, Z.; Talapin, D. V.; Kagan, C. R.; Klimov, V. I.; Rogach, A. L.; Reiss, P.; Milliron, D. J.; et al. Prospects of Nanoscience with Nanocrystals. *ACS Nano* **2015**, *9*, 1012−1057.

(2) Hines, M.; Guyot-Sionnest, P. Synthesis and Characterization of Strongly Luminescing ZnS-Capped CdSe Nanocrystals. *J. Phys. Chem.* **1996**, *100*, 468−471.

(3) Klimov, V. I.; Ivanov, S. A.; Nanda, J.; Achermann, M.; Bezel, I.; McGuire, J. A.; Piryatinski, A. Single-Exciton Optical Gain in Semiconductor Nanocrystals. *Nature* **2007**, *447*, 441−446.

(4) Kundu, J.; Ghosh, Y.; Dennis, A. M.; Htoon, H.; Hollingsworth, J. A. Giant Nanocrystal Quantum Dots: Stable Down-Conversion Phosphors that Exploit a Large Stokes Shift and Efficient Shell-to-Core Energy Relaxation. *Nano Lett.* **2012**, *12*, 3031−3037.

(5) Donega, C. d. M. Synthesis and properties of colloidal heteronanocrystals. *Chem. Soc. Rev.* **2011**, *40*, 1512−1546.

(6) Li, J.; Wang, Y.; Guo, W.; Keay, J.; Mishima, T.; Johnson, M.; Peng, X. Large-Scale Synthesis of Nearly Monodisperse CdSe/CdS Core/Shell Nanocrystals Using Air-Stable Reagents via Successive Ion Layer Adsorption and Reaction. *J. Am. Chem. Soc.* **2003**, *125*, 12567−12575.

(7) Carbone, L.; Nobile, C.; De Giorgi, M.; Sala, F. D.; Morello, G.; Pompa, P.; Hytch, M.; Snoeck, E.; Fiore, A.; Franchini, I. R.; et al. Synthesis and Micrometer-Scale Assembly of Colloidal CdSe/CdS Nanorods Prepared by a Seeded Growth Approach. *Nano Lett.* **2007**, *7*, 2942−2950.

(8) Talapin, D. V.; Nelson, J. H.; Shevchenko, E. V.; Aloni, S.; Sadtler, B.; Alivisatos, A. P. Seeded growth of highly luminescent CdSe/CdS nanoheterostructures with rod and tetrapod morphologies. *Nano Lett.* **2007**, *7*, 2951−2959.

(9) Groeneveld, E.; van Berkum, S.; van Schooneveld, M. M.; Gloter, A.; Meeldijk, J. D.; van den Heuvel, D. J.; Gerritsen, H. C.; de Mello Donega, C. Highly Luminescent (Zn,Cd)Te/CdSe Colloidal Hetero-nanowires with Tunable Electron-Hole Overlap. *Nano Lett.* **2012**, *12*, 749−757.

(10) Fiore, A.; Mastria, R.; Lupo, M. G.; Lanzani, G.; Giannini, C.; Carlino, E.; Morello, G.; De Giorgi, M.; Li, Y.; Cingolani, R.; et al. Tetrapod-Shaped Colloidal Nanocrystals of II-VI Semiconductors Prepared by Seeded Growth. *J. Am. Chem. Soc.* **2009**, *131*, 2274−2282.

(11) Zhong, H.; Scholes, G. D. Shape Tuning of Type II CdTe-CdSe Colloidal Nanocrystal Heterostructures through Seeded Growth. *J. Am. Chem. Soc.* **2009**, *131*, 9170−9171.

(12) Deka, S.; Miszta, K.; Dorfs, D.; Genovese, A.; Bertoni, G.; Manna, L. Octapod-Shaped Colloidal Nanocrystals of Cadmium Chalcogenides via "One-Pot" Cation Exchange and Seeded Growth. *Nano Lett.* **2010**, *10*, 3770−3776.

(13) Cirillo, M.; Aubert, T.; Gomes, R.; Van Deun, R. V.; Emplit, P.; Biermann, A.; Lange, H.; Thomsen, C.; Brainis, E.; Hens, Z. Flash Synthesis of CdSe/CdS Core-Shell Quantum Dots. *Chem. Mater.* **2014**, *26*, 1154−1160.

(14) Drijvers, E.; De Roo, J.; Geiregat, P.; Fehér, K.; Hens, Z.; Aubert, T. Revisited Wurtzite CdSe Synthesis: a Gateway for the Versatile Flash Synthesis of Multi-Shell Quantum Dots and Rods. *Chem. Mater.* **2016**, *28*, 7311−7323.

(15) Liu, H.; Owen, J. S.; Alivisatos, A. P. Mechanistic Study of Precursor Evolution in Colloidal Group II-VI Semiconductor Nanocrystal Synthesis. *J. Am. Chem. Soc.* **2007**, *129*, 305−312.

(16) Steckel, J. S.; Yen, B. K. H.; Oertel, D. C.; Bawendi, M. G. On the Mechanism of Lead Chalcogenide Nanocrystal Formation. *J. Am. Chem. Soc.* **2006**, *128*, 13032−13033.

(17) Abe, S.; Capek, R. K.; De Geyter, B.; Hens, Z. Tuning the Postfocused Size of Colloidal Nanocrystals by the Reaction Rate: From Theory to Application. *ACS Nano* **2012**, *6*, 42−53.

DOI: 10.1021/acs.chemmater.7b00354
Chem. Mater. 2017, 29, 4719−4727

(18) Capek, R. K.; Yanover, D.; Lifshitz, E. Size Control by Rate Control in Colloidal PbSe Quantum Dot Synthesis. *Nanoscale* **2015**, *7*, 5299−5310.
(19) Hendricks, M. P.; Campos, M. P.; Cleveland, G. T.; Jen-La Plante, I.; Owen, J. S. A Tunable Library of Substituted Thiourea Precursors to Metal Sulfide Nanocrystals. *Science* **2015**, *348*, 1226−1230.
(20) van Embden, J.; Jasieniak, J.; Mulvaney, P. Mapping the Optical Properties of CdSe/CdS Heterostructure Nanocrystals: The Effects of Core Size and Shell Thickness. *J. Am. Chem. Soc.* **2009**, *131*, 14299−14309.
(21) Flamee, S.; Cirillo, M.; Abe, S.; De Nolf, K.; Gomes, R.; Aubert, T.; Hens, Z. Fast, High Yield, and High Solid Loading Synthesis of Metal Selenide Nanocrystals. *Chem. Mater.* **2013**, *25*, 2476−2483.
(22) Capek, R. K.; Moreels, I.; Lambert, K.; De Muynck, D.; Zhao, Q.; Vantomme, A.; Vanhaecke, F.; Hens, Z. Optical Properties of Zincblende Cadmium Selenide Quantum Dots. *J. Phys. Chem. C* **2010**, *114*, 6371−6376.
(23) Hens, Z.; Moreels, I. Light Absorption by Colloidal Semiconductor Quantum Dots. *J. Mater. Chem.* **2012**, *22*, 10406−10415.
(24) Angeloni, I.; Raja, W.; Brescia, R.; Polovitsyn, A.; De Donato, F.; Canepa, M.; Bertoni, G.; Proietti Zaccaria, R.; Moreels, I. Disentangling the Role of Shape, Ligands, and Dielectric Constants in the Absorption Properties of Colloidal CdSe/CdS Nanocrystals. *ACS Photonics* **2016**, *3*, 58−67.
(25) Adachi, S. *Optical Constants of Crystalline and Amorphous Semiconductors*; Springer: New York, 1999.
(26) Fritzinger, B.; Capek, R. K.; Lambert, K.; Martins, J. C.; Hens, Z. Utilizing Self-Exchange To Address the Binding of Carboxylic Acid Ligands to CdSe Quantum Dots. *J. Am. Chem. Soc.* **2010**, *132*, 10195−10201.
(27) Ithurria, S.; Talapin, D. V. Colloidal Atomic Layer Deposition (c-ALD) using Self-Limiting Reactions at Nanocrystal Surface Coupled to Phase Transfer between Polar and Nonpolar Media. *J. Am. Chem. Soc.* **2012**, *134*, 18585−18590.
(28) Bladt, E.; van Dijk-Moes, R. J. A.; Peters, J.; Montanarella, F.; de Mello Donega, C. d. M.; Vanmaekelbergh, D.; Bals, S. Atomic Structure of Wurtzite CdSe (Core)/CdS (Giant Shell) Nanobullets Related to Epitaxy and Growth. *J. Am. Chem. Soc.* **2016**, *138*, 14288−14293.
(29) Gomes, R.; Hassinen, A.; Szczygiel, A.; Zhao, Q.; Vantomme, A.; Martins, J. C.; Hens, Z. Binding of Phosphonic Acids to CdSe Quantum Dots: A Solution NMR Study. *J. Phys. Chem. Lett.* **2011**, *2*, 145−152.
(30) Talapin, D.; Mekis, I.; Gotzinger, S.; Kornowski, A.; Benson, O.; Weller, H. CdSe/CdS/ZnS and CdSe/ZnSe/ZnS Core-Shell-Shell Nanocrystals. *J. Phys. Chem. B* **2004**, *108*, 18826−18831.
(31) Reiss, P.; Bleuse, J.; Pron, A. Highly Luminescent CdSe/ZnSe Core/Shell Nanocrystals of Low Size Dispersion. *Nano Lett.* **2002**, *2*, 781−784.
(32) Talapin, D.; Rogach, A.; Haase, M.; Weller, H. Evolution of an Ensemble of Nanoparticles in a Colloidal Solution: Theoretical Study. *J. Phys. Chem. B* **2001**, *105*, 12278−12285.
(33) Abe, S.; Capek, R. K.; De Geyter, B.; Hens, Z. Reaction Chemistry/Nanocrystal Property Relations in the Hot Injection Synthesis, the Role of the Solute Solubility. *ACS Nano* **2013**, *7*, 943−949.

DOI: 10.1021/acs.chemmater.7b00354
Chem. Mater. 2017, 29, 4719−4727